Enhanced Strain Coupling of Nitrogen-Vacancy Spins to Nanoscale Diamond Cantilevers

Srujan Meesala, Young-Ik Sohn, Haig A. Atikian, Samuel Kim,[*] Michael J. Burek, Jennifer T. Choy,[†] and Marko Lončar[‡]

John A. Paulson School of Engineering and Applied Sciences, Harvard University, 29 Oxford Street, Cambridge, Massachusetts 02138, USA

(Received 6 November 2015; published 18 March 2016)

Nitrogen-vacancy (NV) centers can couple to confined phonons in diamond mechanical resonators via the effect of lattice strain on their energy levels. Access to the strong spin-phonon coupling regime with this system requires resonators with nanoscale dimensions in order to overcome the weak strain response of the NV ground-state spin sublevels. In this work, we incorporate photostable NVs in diamond cantilevers with lateral dimensions of a few hundred nanometers. Coupling of the NV ground-state spin to the mechanical mode is detected in electron spin resonance, and its temporal dynamics are measured via spin echo. Our small mechanical-mode volume leads to a $10\times - 100\times$ enhancement in the spin-phonon coupling strength over previous NV-strain coupling demonstrations. This is an important step towards strong spin-phonon coupling, which can enable phonon-mediated quantum-information processing and quantum metrology.

DOI: 10.1103/PhysRevApplied.5.034010

I. INTRODUCTION

Quantum two-level systems (qubits) strongly coupled to mechanical resonators can function as hybrid quantum systems with several potential applications in quantum-information science [1–3]. The physics of these systems can be well described with the tools of cavity quantum electrodynamics (cQED), in which an atom is strongly coupled to photons in an electromagnetic cavity. Such qubit–mechanical-mode interactions are key ingredients for quantum logic with ion traps [4] and have been used to generate nonclassical states of a mechanical resonator coupled to a superconducting qubit [5]. Furthermore, phonons or mechanical vibrations couple to a wide variety of well-studied quantum systems and are, therefore, considered a promising means to coherently interface qubits across disparate energy scales [1–3]. In the context of solid-state emitters, mechanical hybrid systems were first proposed [6] and subsequently demonstrated [7,8] with the electronic states of quantum dots. Such a mechanical hybrid quantum system with negatively charged nitrogen-vacancy [NV(−), hereafter referred to as NV] centers in diamond, in particular, would benefit from their long spin-coherence times [9]. It has been proposed that, in the strong spin-phonon coupling regime, phonons can be used to mediate quantum-state transfer and generate effective interactions between NV spins [10]. Strong coupling of a NV spin ensemble to a mechanical resonator can also be used to generate squeezed spin states [11], which can enable high-sensitivity magnetometry [12].

Seminal experiments on coupling NV spins to mechanical oscillators relied on magnetic-field gradients [13–15]. More recently, owing to the development of single-crystal diamond nanofabrication techniques [16–22], the effect of lattice strain on the NV ground-state spin sublevels has been exploited to couple NVs to mechanical modes of diamond cantilevers [23–25] and bulk acoustic-wave resonators fabricated on diamond [26–28]. Strain-mediated coupling is experimentally elegant, since its origin is intrinsic to a monolithic device, and it does not involve functionalization of mechanical resonators or precise and stable positioning of magnetic tips very close to a diamond chip. However, current demonstrations are far from the strong-coupling regime due to the small spin-phonon coupling strength provided by strain from relatively large mechanical resonators. As a result of the large device size, the NVs in previous experiments [23–25] either are situated in bulk diamond or are sufficiently distant from etched diamond surfaces. This bulklike nature of the NVs mitigates experimental challenges with photostability of their charge state, which are typically observed in fabricated diamond nanostructures [29–31]. However, diamond devices with nanoscale dimensions are essential to achieve highly confined strain fields and reach strong coupling. In this work, we present an important step in this direction by incorporating photostable NVs in a diamond cantilever with nanoscale transverse dimensions and demonstrate a

[*]Present address: Research and Exploratory Development Department, Johns Hopkins University Applied Physics Laboratory, Laurel, MD 20723, USA.

[†]Present address: Draper Laboratory, 555 Technology Square, Cambridge, MA 02139, USA.

[‡]loncar@seas.harvard.edu

single-phonon coupling rate of approximately 2 Hz from the dispersive interaction of NV spins with the resonator. This is an approximately $10\times - 100\times$ improvement over existing NV-strain coupling demonstrations [23,24]. In our experiments, we first detect the effect of driven cantilever motion on NVs as a broadening of their electron spin resonance (ESR) signal and, through follow-up measurements, establish this to be strain-mediated coupling to the mechanical mode of interest. Subsequently, we use spin echo to probe the temporal dynamics of NVs in the cantilever and precisely measure the spin-phonon coupling rate. In the conclusion, we discuss subsequent device-engineering options to further improve this coupling strength by approximately $100\times$ and reach the strong-coupling regime.

II. REQUIREMENTS FOR STRONG SPIN-PHONON COUPLING

In analogy with atom-photon interactions in cQED, the key requirement for applications that rely on strong qubit-phonon coupling is that the cooperativity of the interaction exceed unity [13]:

$$C = \frac{g^2}{n_{\mathrm{th}}\kappa\gamma} > 1. \tag{1}$$

Here, g is the coupling rate between the qubit levels due to a single phonon in the mechanical mode, n_{th} is the thermal phonon occupation of the mechanical mode of interest, κ is the intrinsic mechanical damping rate, and γ is the qubit-dephasing rate. For a strain-mediated linear coupling, the single-phonon coupling rate is given by $g = d\epsilon_{\mathrm{ZPM}}$, where ϵ_{ZPM} is the strain due to zero point motion and d is the strain susceptibility, an intrinsic property of the qubit energy levels. d is analogous to the dipole moment of an electric dipole and reveals the frequency shift of the transition per unit of strain. The spin-triplet ground state of the NV has a relatively small $d \approx 10$–20 GHz/strain [23,24], since the three spin sublevels share the same orbital wave function. The effect of strain on these levels is proposed to be due to a small perturbative mixing of the ground- and excited-state orbitals by spin-orbit coupling [32] and a change in the spin-spin interaction energy in the deformed ground-state orbital [33]. Thus, engineering the mechanical mode to provide large ϵ_{ZPM} is essential to achieve large g. For instance, for the fundamental out-of-plane flexural mode of a cantilever of width w, thickness t, and length l, we can use the Euler-Bernoulli beam theory [34] to show that

$$\epsilon_{\mathrm{ZPM}} \propto \frac{1}{\sqrt{l^3 w}}. \tag{2}$$

This sharp inverse scaling of ϵ_{ZPM} with cantilever dimensions highlights the importance of working with small resonators. It is analogous to the $1/\sqrt{V_{\mathrm{eff}}}$ scaling of the single-photon Rabi frequency in cQED, where V_{eff} is the electromagnetic mode volume. To achieve the strong-coupling condition in Eq. (1), assuming a NV spin-coherence time $T_2 = 100$ ms, a mechanical quality factor $Q = \omega/\kappa = 10^6$, and cryogenic operation temperatures (4 K or lower), cantilevers of width $w \sim 50$–100 nm and length $l \sim 1\ \mu$m (corresponding mechanical frequency, $\omega_m \approx$ few hundred MHz) that provide $g \approx$ few hundred Hz are required. At these estimated length scales, the proximity to surfaces deteriorates the photostability of the NV charge state in nanostructures fabricated by plasma etching, which is the workhorse technique for diamond nanofabrication.

III. DEVICE FABRICATION AND EXPERIMENTAL SETUP

Incorporating photostable NV centers close to surfaces [35,36], particularly in nanostructures with small transverse dimensions such as nanophotonic cavities [29,30], has been found to be a considerably challenging task in recent years. To prevent charge-state blinking and photoionization of NVs under optical excitation [31], high-quality surfaces with low defect density and appropriate surface termination are necessary. Recent advances in annealing and surface-passivation procedures [37] have significantly improved the ability to retain photostable NV centers generated by ion implantation even after the fabrication of nanostructures around them [38]. We combine these methods with our angled reactive ion-etching fabrication scheme [18] (details discussed in Appendix A) to repair etch-induced damage and generate photostable NVs in diamond nanocantilevers with a triangular cross section [Figs. 1(a) and 1(b)]. The NVs are situated at a depth $d = 94$ nm from the top surface of the cantilever [inset in Fig. 1(c)] and are at a distance of 65 nm from the etched sidewalls of the cantilevers. Previously, we have demonstrated high Q-factor mechanical modes (Q approaching 100 000) with frequencies ranging from <1 MHz to tens of MHz in cantilevers and doubly clamped nanobeams fabricated using the same angled etching scheme [39].

Our measurements are carried out at high vacuum (10^{-5} torr) and room temperature in a vacuum chamber with a view port underneath a homebuilt scanning confocal microscope for addressing NV centers. Microwaves for ESR measurements are delivered with a wire bond positioned close to the devices of interest. The diamond chip is mounted on a piezoactuator for resonant actuation of cantilevers. Mechanical-mode spectroscopy performed via optical interferometry [40] is used to characterize the modes of the cantilevers. For the experiments described in this paper, we used a triangular cross-section cantilever with $w = 580$ nm, $t = 170$ nm, and $l = 19\ \mu$m. The mechanical mode of interest in the measurements that follow [Fig. 1(c)] is the fundamental out-of-plane

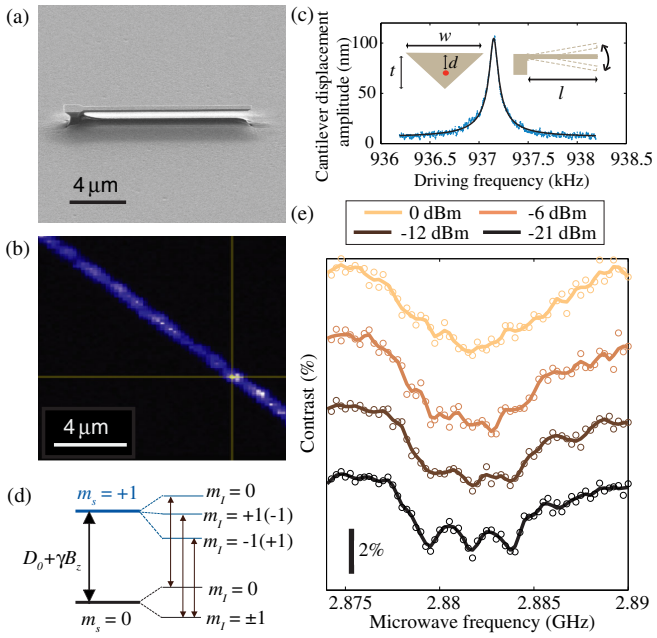

FIG. 1. (a) Representative scanning electron microscope image of the angle-etched diamond cantilevers used. (b) Representative confocal microscope scan of a section of the cantilever showing fluorescence from NV centers. (c) Driven response of the fundamental out-of-plane flexural mode (right inset) of the triangular cross-section (left inset) cantilevers studied in this work measured by optical interferometry. For this particular device, we have $w = 580$ nm, $t = 170$ nm, and $l = 19$ μm. NV centers are situated at a depth $d = 94$ nm. The mode frequency is 937.2 kHz, and it has a Q factor of 10 000. Measurements are taken in high vacuum (10^{-5} torr) at room temperature. (d) Hyperfine structure of the $m_s = 0$ to $m_s = +1$ electron spin transition in the NV ground state indicating the three allowed microwave transitions. (e) ac strain-induced broadening of the $m_s = 0$ to $m_s = +1$ hyperfine transitions near the clamp of the cantilever with gradually increasing mechanical amplitude. The mechanical mode is inertially driven at its resonance frequency with a piezostack in all measurements. Open circles indicate measured data, and smoothed solid lines serve as a guide to the eye. The legend shows values of piezodrive power for each measurement. 0 dBm of drive power corresponds to an amplitude of 559 ± 2 nm at the tip of the cantilever.

flexural mode, which is found to have a frequency $\omega_m = 2\pi \times 937.2$ kHz and a quality factor $Q \sim 10\,000$.

IV. AC STRAIN-INDUCED ESR BROADENING

The effect of lattice strain on the $S = 1$ ground state of the NV center is described by the Hamiltonian [11,23,24,32]

$$H = D_0 S_z^2 + \gamma \mathbf{S}\cdot\mathbf{B} + d_\parallel \epsilon_{zz} S_z^2 - \frac{d_\perp}{2}[\epsilon_+ S_+^2 + \epsilon_- S_-^2]. \quad (3)$$

Here S_i are the $S = 1$ Pauli spin operators. $D_0 = 2.87$ GHz is the zero-field splitting between $m_s = 0$ and $m_s = \pm 1$ levels due to spin-spin interaction, and $\gamma = 2.8$ MHz/G is the gyromagnetic ratio for the NV ground state. At small B fields ($\ll D_0/\gamma$), the NV axis is the spin-quantization axis (z axis in the above Hamiltonian). $d_\parallel$ and $d_\perp$ are, respectively, the axial and transverse strain susceptibilities defined with reference to the NV axis. ϵ_{ii} are the diagonal strain-tensor components defined in the basis of the NV, and $\epsilon_\pm = \epsilon_{xx} \pm i\epsilon_{yy}$. The perturbative strain terms lead to frequency shifts in the $m_s = \pm 1$ levels, respectively given by

$$\Delta\omega_\pm = d_\parallel \epsilon_\parallel \pm \sqrt{(\gamma B_z)^2 + (d_\perp \epsilon_\perp)^2}. \quad (4)$$

Here, $\epsilon_\perp$ denotes the total transverse strain $\sqrt{\epsilon_{xx}^2 + \epsilon_{yy}^2}$. Physically, Eq. (4) reveals that axial strain leads to a linear modification of the zero-field splitting, while transverse strain mixes the $m_s = \pm 1$ states, thereby causing a quadratic splitting between them. In a mechanical resonator driven at the frequency ω_m, the local strain components $\epsilon_\parallel$ and $\epsilon_\perp$ oscillate at the frequency ω_m. The classical effect of driving the mechanical mode on the NV ground state is frequency modulation of the two transitions between $m_s = 0$ and $m_s = \pm 1$ levels. From the strain susceptibilities measured in Ref. [8] and finite-element calculations on our structures, we anticipate a frequency modulation comparable to the ESR linewidth, when the mechanical mode is driven to an amplitude of approximately 500 nm.

At the chosen nitrogen-ion implantation density, we expect approximately 10 NV centers within our confocal laser spot. ESR measurements are performed on such a NV ensemble at a fixed position in the cantilever, and, simultaneously, the flexural mode shown in Fig. 1(c) is driven by supplying a rf voltage to the piezoactuator at the resonance frequency ω_m. A small static magnetic field $B_z = 4$ G is applied with a bar magnet placed outside the cryostat, and only the $m_s = 0$ to $m_s = +1$ transition is probed. The external magnetic field is aligned exactly vertically to ensure that all four NV classes experience the same projection B_z along their respective axes. The cantilever itself is fabricated such that its long axis is aligned to the $\langle 100\rangle$ crystal axis to within a few degrees as determined by electron backscatter diffraction. As a result, all four NV classes are symmetrically aligned with respect to the dominant strain component of the flexural mode, which occurs along the cantilever long axis. Thus, at a given location in the cantilever, all four NV classes experience the same axial and transverse strain amplitudes and, hence, experience identical transition frequency modulation. The effects of inhomogeneous coupling strength due to implantation straggle and varying the lateral position within the confocal laser spot are addressed in Appendix B. Low microwave power is used to prevent power broadening and retain near-native linewidths in the ESR.

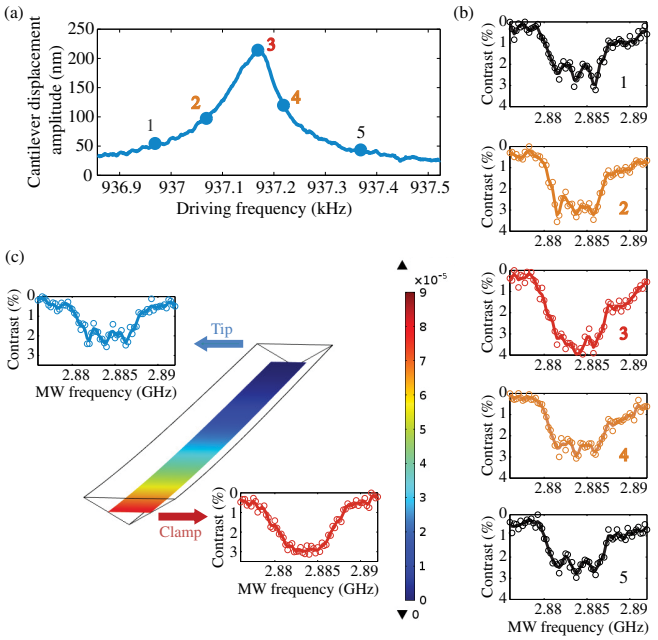

FIG. 2. (a) Driven response of the cantilever measured by optical interferometry at a piezodrive power of −12 dBm. The drive frequencies used for frequency-dependent broadening measurements are indicated with numbers 1–5. (b) ESR spectra at the same location in the cantilever at mechanical drive frequencies 1–5 indicated in (a). (c) ESR spectra at the tip and clamp of the cantilever for −6 dBm of drive power. The strain profile of the mechanical mode from a FEM simulation for the corresponding displacement amplitude is also shown. Open circles in each ESR spectrum are measured data, and smoothed lines serve as a guide to the eye

Figure 1(e) shows ESR spectra at the same location in the cantilever for a progressively increasing mechanical amplitude. At the lowest piezodrive power of −21 dBm, we observe three dips spaced equally by 2.2 MHz corresponding to the hyperfine structure arising from the interaction between the NV electron spin and the ^{14}N nuclear spin [Fig. 1(d)]. This is found to be identical to the ESR spectrum with no piezodrive (not shown). For each of the hyperfine transitions, we measure a linewidth of approximately 2 MHz. As the piezodrive power is increased to −12 dBm, we observe a broadening of the hyperfine features to the point where the hyperfine structure is barely resolvable. At −6 dBm, the hyperfine structure is washed out, and at 0 dBm, the overall ESR dip is even broader. Such a broadening of the ESR signal with a progressively larger mechanical amplitude is expected, since the measurement sequence involves dwelling at each microwave frequency sample for many ($> 10^6$) cycles of the mechanical oscillation period. As a result, we would expect to average over the ac modulation of the microwave transition and detect an overall broadening determined by the modulation amplitude.

To verify that the ESR broadening arises from the mechanical mode, we perform the same measurement at a fixed piezodrive power of −12 dBm and multiple drive frequencies around resonance. The slight asymmetry in the driven mechanical response [Fig. 2(a)] can be attributed to the onset of a Duffing-type nonlinearity at this drive power. When driven far off the mechanical resonance as in points 1 and 5 in Fig. 2(b), the ESR spectrum retains three clear hyperfine dips with linewidths close to the native linewidth. At smaller detunings as in points 2 and 4 in Fig. 2(b), we observe a broadening of the individual hyperfine features. When driven exactly on resonance as in point 3 in Fig. 2(d), the hyperfine features are on the verge of being washed out. Thus, the ESR-broadening effect follows the frequency response of the mechanical mode. To further confirm that this is a strain-induced effect, we repeat the measurement at multiple points along the length of the cantilever for a fixed piezodrive power of −6 dBm. From the strain profile of the flexural mode [Fig. 2(c)], we expect a roughly linear variation in ac strain amplitude from its maximum value near the clamp of the cantilever to zero at the tip of the cantilever. This effect is observed in the form of ESR broadening for NVs near the clamp and retention of native linewidths for NVs at the tip [Fig. 2(c)].

V. TEMPORAL DYNAMICS OF THE MECHANICALLY DRIVEN SPIN

The ESR-broadening measurements in Figs. 1(e) and 2 provide strong evidence of strain from the driven mechanical-mode coupling to the NV spin. From the washing out of hyperfine structure in the measurements, we can deduce driven coupling rates of the order of the hyperfine splitting (2.2 MHz). In order to probe the temporal dynamics of the NV spin due to mechanical motion and precisely measure the coupling strength, we employ spin-echo measurements. It has been shown in previous demonstrations that the two distinct modes of level shifts generated by axial and transverse strain can be used to achieve dispersive [23] and resonant interactions [25–28] of the spin with mechanical motion, respectively. In our work, the frequency of our mechanical mode (approximately 1 MHz) is smaller than the ESR linewidth, and we focus on the dispersive regime provided by axial strain. We apply a moderate static magnetic field and suppress the effect of transverse strain to first order as evinced by Eq. (4). In this regime, if we work with the effective qubit defined by the $m_s = 0$ and $m_s = +1$ levels, the driven motion of the mechanical resonator can modulate the phase of our effective qubit at the frequency ω_m, analogous to an ac magnetic field. This is described by the time-dependent Hamiltonian

$$H_{\rm int}(t) = 2\pi G \cos(\omega_m t + \phi)\sigma_z. \tag{5}$$

Here $G = d_{\parallel}\epsilon_{zz}$ is the ac strain coupling rate from the driven motion, ϕ is an arbitrary phase offset, and σ_z is the corresponding $S = 1/2$ Pauli spin operator.

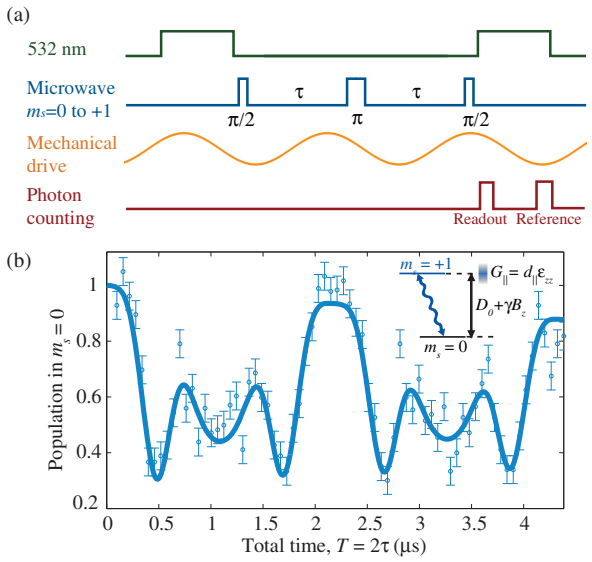

FIG. 3. (a) Experimental pulse sequence for spin-echo measurement of dispersive spin-cantilever interaction due to axial strain. (b) Spin-echo signal from NVs in the cantilever at a piezodrive power of 0 dBm (tip amplitude of 559 ± 2 nm) for the mode at $\omega_m = 923.4$ kHz, showing two periods of the modulation due to axial strain coupling. The solid line is a fit to Eq. (6). Vertical error bars correspond to photon shot noise in the measurement. The inset shows a schematic of the dispersive interaction between the qubit and mechanical mode due to axial strain.

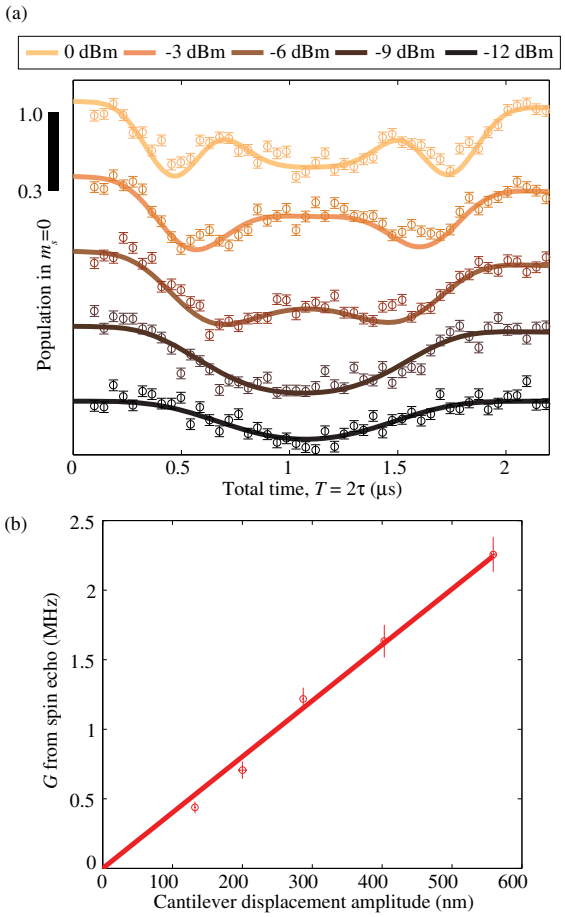

FIG. 4. (a) Spin echo at the same location in the cantilever for varying piezodrive powers, offset along the y axis. One period of the signal is plotted in each case. Solid lines are fits to the zero-order Bessel function form indicated in the text, and vertical error bars correspond to photon shot noise. The scale bar on the side is a guide for the y axis indicating the maximum (1.0) and minimum (0.3) possible population in $m_s = 0$ as dictated by Eq. (6). The legend on the right side indicates the piezodrive powers used for each measurement. (b) Variation of the driven spin-phonon coupling rate due to axial strain (G) with the calibrated displacement amplitude of the mechanical mode. The five data points correspond to the piezodrive powers used in (a) in increasing order. Vertical error bars correspond to the error in each G estimate from fitting to the spin-echo function given by Eq. (6). The solid line is a linear fit, which yields $dG/dx = 4.02 \pm 0.40$ kHz/nm.

In our spin-echo measurements, we apply an external static magnetic field $B_z = 27$ G. As in the case of ESR measurements, the magnetic field is aligned to ensure equal Zeeman splittings for all four NV orientations. Our experimental sequence is shown in Fig. 3(a), wherein the piezodrive signal, and hence the strain field, has an arbitrary phase ϕ with respect to the microwave pulses that varies over multiple iterations of the sequence. The spin-echo signal obtained from this measurement [Fig. 3(b)] at a piezodrive power of 0 dBm shows a periodicity corresponding to twice the time period of the mechanical mode. The theoretically expected spin-echo signal in this measurement has the form of a zero-order Bessel function with a periodic argument [13,23]:

$$p(2\tau) = \frac{1}{2}\left\{1 + e^{-(2\tau/T_2)^3} J_0\left[\frac{8\pi G}{\omega_m}\sin^2\left(\frac{\omega_m \tau}{4}\right)\right]\right\}. \quad (6)$$

The exponential damping term multiplying the periodic function corresponds to the dephasing of the NV electron spin due to interactions with the surrounding ^{13}C nuclear spin bath in diamond, and T_2 is the dephasing time [41]. In our experiments, $T_2 \gg$ the mechanical oscillation period $(2\pi/\omega_m)$, and the effect of spin decoherence is relatively small. A fit to Eq. (6) yields $\omega_m = 2\pi \times 918.7 \pm 5.6$ kHz, which is in reasonable agreement with the driving frequency of 923.4 kHz used in the experiment. The extracted driven coupling rate $G = 2.10 \pm 0.07$ MHz is of the order of the hyperfine splitting as observed in our ESR-broadening measurements.

Finally, we perform spin-echo measurements at the same location on the cantilever for varying piezodrive powers [Fig. 4(a)]. The no-drive spin-echo signal (not shown) is flat, indicating that this measurement is not sensitive to the thermal motion of the cantilever mode (estimated to have an amplitude of 0.53 nm). As the cantilever is driven, the spin-echo signal begins to show a dip when the evolution

time 2τ equals the mechanical oscillation period ($2\pi/\omega_m$). At larger amplitudes, the spin precesses by more than one full rotation on the equator of the Bloch sphere, and we observe higher-order fringes within one period of the signal. These drive-power-dependent measurements directly allow us to verify that the axial strain coupling is linear in the displacement amplitude of the cantilever measured by optical interferometry [Fig. 4(b)]. From the linear fit, we infer a displacement sensitivity $dG/dx = 4.02 \pm 0.40$ kHz/nm. The cantilever oscillation amplitudes in these driven coupling measurements correspond to $n \sim 10^{12}$ phonons in the mechanical mode. In order to estimate the single-phonon coupling strength g (where $G = \sqrt{n}g$), we multiply the above displacement sensitivity dG/dx with the zero point motion amplitude ($x_{\mathrm{ZPM}} = \sqrt{\hbar/2m_{\mathrm{eff}}\omega_m}$) estimated from the measured cantilever dimensions and account for the NV position in the cantilever. This yields a single-phonon coupling strength of $g = 1.84 \pm 0.18$ Hz for this device. Compared with previous demonstrations of NV-strain coupling, this is about 2 orders of magnitude larger than that measured in Ref. [23] and an order of magnitude larger than that in Refs. [24,25]. Furthermore, this marks the extension of strain-mediated NV coupling into the nanoscale regime in which addressing the effects of surfaces on NVs is critical.

VI. CONCLUSION AND OUTLOOK FOR STRONG COUPLING

In conclusion, we demonstrate nanoscale diamond cantilevers for strain-mediated coupling of NV spins to mechanical resonators. By generating photostable NVs in plasma-etched devices with nanoscale dimensions, we show a significant improvement in the single-phonon coupling strength compared to previous work with mechanical modes at similar frequencies. Shorter cantilevers will boost g even further according to the scaling in Eq. (2). This will also increase the mechanical frequencies and allow operation in the sideband-resolved regime with access to the resonant spin-phonon interaction provided by transverse strain coupling [25–28]. As suggested by our estimates in the introduction, nanostructures that allow strong coupling have mechanical frequencies in the few hundreds of megahertz range. Since piezoactuation used in this work is not extendable to such high frequencies, this also necessitates the engineering of actuation and transduction schemes around these diamond nanomechanical devices. Our recent efforts address the goal of developing high-frequency nanomechanical resonators in single-crystal diamond that can be actuated and transduced both electrically and optically. Dynamic actuation and transduction of single-crystal diamond resonators up to frequencies of 50 MHz is achieved with dielectric gradient forces in Ref. [42] and up to 6 GHz is achieved by using cavity optomechanics in Ref. [43]. Given these developments, we anticipate that the major engineering challenge for strain-mediated strong spin-phonon coupling will be the ability to maintain photostable NVs in nanostructures with extremely small widths. The inclusion of a postfabrication high-temperature annealing process will allow us to shrink our lateral device dimensions even further (the current state of the art being nanobeams with $w \approx 200$ nm in Ref. [38]). A remaining challenge is the demand for high Q factors in the $10^5 - 10^6$ range from small resonators, which are usually difficult to engineer for high Q [44].

However, these system-engineering requirements can be less daunting for magnetometry applications that can benefit from a NV ensemble coupled to a mechanical resonator [11]. In particular, collective enhancement from a dense spin ensemble can boost the cooperativity by a factor of the number of spins N [45], allowing one to work with device dimensions more favorable for NV photostability and high mechanical Q factors. Alternatively, since the technique of strain-mediated coupling is fairly general, the same devices may be used, but with a different qubit, whose energy levels have a larger strain response. Potential candidates include the NV center excited electronic state [46,47] and the orbital ground states of the silicon-vacancy (SiV) center [48], both of which have 4–5 orders of magnitude larger strain susceptibility than the NV ground-state spin sublevels.

ACKNOWLEDGMENTS

The authors thank Ruffin Evans, Nathalie de Leon, Kristiaan de Greve, and Yiwen Chu for sharing diamond annealing and surface treatment procedures and acknowledge Arthur Safira, Vivek Venkataraman, and Mikhail Lukin for helpful discussions. This work was supported by DARPA QuASAR (Grant No. HR0011-11-C-0073), STC Center for Integrated Quantum Materials (NSF Grant No. DMR-1231319), and ONR MURI on Quantum Optomechanics (Grant No. N00014-15-1-2761). H. A. A. and M. J. B. were supported in part by the Natural Science and Engineering Council (NSERC) of Canada and the Harvard Quanum Optics Center (HQOC). This work was performed in part at the Center for Nanoscale Systems (CNS), a member of the National Nanotechnology Infrastructure Network (NNIN), which is supported by the National Science Foundation under NSF Grant No. ECS-0335765. CNS is part of Harvard University.

S. M. and Y.-I. S. contributed equally to this work.

APPENDIX A: SAMPLE PREPARATION

Single-crystal electronic-grade bulk diamond chips (4 mm × 4 mm) from Element Six Ltd. are implanted with ^{14}N ions at an implantation energy of 75 keV and a dose of $6 \times 10^{11}/\mathrm{cm}^2$. This yields an expected depth of 94 ± 19 nm calculated using software from Stopping and Range of Ions in Matter (SRIM). Subsequently, NVs are created by

annealing the samples in high vacuum ($<5\times10^{-7}$ torr). The temperature ramp sequence described in Ref. [37] is followed with a final temperature of 1200 °C, which is maintained for 2 h. After the anneal, the samples are cleaned in a 1:1:1 boiling mixture of sulfuric, nitric, and perchloric acids to remove a few nanometers of graphite generated on the surface from the anneal. Cantilevers are then patterned using e-beam lithography and etched using our angled etching scheme [18]. Postfabrication, we repeat the triacid cleaning treatment to partially repair etch-induced damage and perform a piranha clean to ensure a predominantly oxygen-terminated diamond surface (diagnosed by x-ray photoelectron spectroscopy), which is beneficial for NV photostability [36–38].

APPENDIX B: ENSEMBLE EFFECTS

We address the effect of inhomogeneous coupling strengths in ac strain coupling measurements on a NV ensemble. The width of our confocal laser spot approximately 560 nm is about 40 times smaller than the length of the cantilever (19 μm). Taking into account the roughly linear variation of strain along the length of the cantilever, we expect an approximately 2% variation in coupling strength within the confocal spot due to lateral distribution of NVs. This is less than the order of the error in the fitted estimate for G. Now, we consider the more significant effect of ion-implantation straggle, which is expected to be approximately 20% for our chosen NV depth from SRIM. Upon fitting the experimental spin-echo signal to the formula in Eq. (6) convolved with a 20% Gaussian straggle in G, we notice that our estimate for G does not change to within the error bars. We believe that this is because the level of photon shot noise in our measurement (±0.05 error in spin-population estimates) does not allow us to ultimately resolve the effect of any inhomogeneity in G across the ensemble.

[1] M. Wallquist, K. Hammerer, P. Rabl, M. Lukin, and P. Zoller, Hybrid quantum devices and quantum engineering, Phys. Scr. **T137**, 014001 (2009).

[2] K. Stannigel, P. Rabl, A. S. Sørensen, P. Zoller, and M. D. Lukin, Optomechanical Transducers for Long-Distance Quantum Communication, Phys. Rev. Lett. **105**, 220501 (2010).

[3] K. Stannigel, P. Rabl, A. S. Sørensen, M. D. Lukin, and P. Zoller, Optomechanical transducers for quantum-information processing, Phys. Rev. A **84**, 042341 (2011).

[4] D. Leibfried, B. DeMarco, V. Meyer, D. Lucas, M. Barrett, J. Britton, W. M. Itano, B. Jelenkovic, C. Langer, T. Rosenband, and D. J. Wineland, Experimental demonstration of a robust, high-fidelity geometric two ion-qubit phase gate, Nature (London) **422**, 412 (2003).

[5] A. D. O'Connell, M. Hofheinz, M. Ansmann, Radoslaw C. Bialczak, M. Lenander, Erik Lucero, M. Neeley, D. Sank, H. Wang, M. Weides, J. Wenner, J. M. Martinis, and A. N. Cleland, Quantum ground state and single-phonon control of a mechanical resonator, Nature (London) **464**, 697 (2010).

[6] I. Wilson-Rae, P. Zoller, and A. Imamoğlu, Laser Cooling of a Nanomechanical Resonator Mode to its Quantum Ground State, Phys. Rev. Lett. **92**, 075507 (2004).

[7] M. Metcalfe, S. M. Carr, A. Muller, G. S. Solomon, and J. Lawall, Resolved Sideband Emission of InAs/GaAs Quantum Dots Strained by Surface Acoustic Waves, Phys. Rev. Lett. **105**, 037401 (2010).

[8] I. Yeo, P-L. de Assis, A. Gloppe, E. Dupont-Ferrier, P. Verlot, N. S. Malik, E. Dupuy, J. Claudon, J-M. Gérard, A. Auffèves, G. Nogues, S. Seidelin, J-Ph. Poizat, O. Arcizet, and M. Richard, Strain-mediated coupling in a quantum dot mechanical oscillator hybrid system, Nat. Nanotechnol. **9**, 106 (2014).

[9] N. Bar-Gill, L. M. Pham, A. Jarmola, D. Budker, and R. L. Walsworth, Solid-state electronic spin coherence time approaching one second, Nat. Commun. **4**, 1743 (2013).

[10] P. Rabl, S. J. Kolkowitz, F. H. L. Koppens, J. G. E. Harris, P. Zoller, and M. D. Lukin, A quantum spin transducer based on nanoelectromechanical resonator arrays, Nat. Phys. **6**, 602 (2010).

[11] S. D. Bennett, N. Y. Yao, J. Otterbach, P. Zoller, P. Rabl, and M. D. Lukin, Phonon-Induced Spin-Spin Interactions in Diamond Nanostructures: Application to Spin Squeezing, Phys. Rev. Lett. **110**, 156402 (2013).

[12] R. J. Sewell, M. Koschorreck, M. Napolitano, B. Dubost, N. Behbood, and M. W. Mitchell, Magnetic Sensitivity beyond the Projection Noise Limit by Spin Squeezing, Phys. Rev. Lett. **109**, 253605 (2012).

[13] S. Kolkowitz, A. C. Bleszynski Jayich, Q. P. Unterreithmeier, S. D. Bennett, P. Rabl, J. G. E. Harris, and M. D. Lukin, Coherent sensing of a mechanical resonator with a single-spin qubit, Science **335**, 1603 (2012).

[14] S. Hong, M. S. Grinolds, P. Maletinsky, R. L. Walsworth, M. D. Lukin, and A. Yacoby, Coherent, mechanical control of a single electronic spin, Nano Lett. **12**, 3920 (2012).

[15] O. Arcizet, V. Jacques, A. Siria, P. Poncharal, P. Vincent, and S. Seidelin, A single nitrogen-vacancy defect coupled to a nanomechanical oscillator, Nat. Phys. **7**, 879 (2011).

[16] B. J. M. Hausmann, M. Khan, Y. Zhang, T. M. Babinec, K. Martinick, M. McCutcheon, P. R. Hemmer, and M. Lončar, Fabrication of diamond nanowires for quantum information processing applications, Diamond Relat. Mater. **19**, 621 (2010).

[17] B. J. M. Hausmann, B. Shields, Q. Quan, P. Maletinsky, M. McCutcheon, J. T. Choy, T. M. Babinec, A. Kubanek, A. Yacoby, M. D. Lukin, and M. Lončar, Integrated diamond networks for quantum nanophotonics, Nano Lett. **12**, 1578 (2012).

[18] M. J. Burek, N. P. de Leon, B. J. Shields, B. J. M. Hausmann, Y. Chu, Q. Quan, A. S. Zibrov, H. Park, M. D. Lukin, and M. Lončar, Free-standing mechanical and photonic nanostructures in single-crystal diamond, Nano Lett. **12**, 6084 (2012).

[19] P. Ovartchaiyapong, L. M. A. Pascal, B. A. Myers, P. Lauria, and A. C. Bleszynski Jayich, High quality factor single-crystal diamond mechanical resonators, Appl. Phys. Lett. **101**, 163505 (2012).

[20] Y. Tao, J. M. Boss, B. A. Moores, and C. L. Degen, Single-crystal diamond nanomechanical resonators with quality factors exceeding one million, Nat. Commun. **5**, 3638 (2014).
[21] B. Khanaliloo, M. Mitchell, A. C. Hryciw, and P. E. Barclay, High-Q/V monolithic diamond microdisks fabricated with quasi-isotropic etching, Nano Lett. **15**, 5131 (2015).
[22] B. Khanaliloo, H. Jayakumar, A. C. Hryciw, D. P. Lake, H. Kaviani, and P. E. Barclay, Single Crystal Diamond Nanobeam Waveguide Optomechanics, Phys. Rev. X **5**, 041051 (2015).
[23] P. Ovartchaiyapong, K. W. Lee, B. A. Myers, and A. C. Bleszynski Jayich, Dynamic strain-mediated coupling of a single diamond spin to a mechanical resonator, Nat. Commun. **5**, 4429 (2014).
[24] J. Teissier, A. Barfuss, P. Appel, E. Neu, and P. Maletinsky, Strain Coupling of a Nitrogen-Vacancy Center Spin to a Diamond Mechanical Oscillator, Phys. Rev. Lett. **113**, 020503 (2014).
[25] A. Barfuss, J. Teissier, E. Neu, A. Nunnenkamp, and P. Maletinsky, Strong mechanical driving of a single electron spin, Nat. Phys. **11**, 820 (2015).
[26] E. R. MacQuarrie, T. A. Gosavi, N. R. Jungwirth, S. A. Bhave, and G. D. Fuchs, Mechanical Spin Control of Nitrogen-Vacancy Centers in Diamond, Phys. Rev. Lett. **111**, 227602 (2013).
[27] E. R. MacQuarrie, T. A. Gosavi, A. M. Moehle, N. R. Jungwirth, S. A. Bhave, and G. D. Fuchs, Coherent control of a nitrogen-vacancy center spin ensemble with a diamond mechanical resonator, Optica **2**, 233 (2015).
[28] E. R. MacQuarrie, T. A. Gosavi, S. A. Bhave, and G. D. Fuchs, Continuous dynamical decoupling of a single diamond nitrogen-vacancy center spin with a mechanical resonator, Phys. Rev. B **92**, 224419 (2015).
[29] B. J. M. Hausmann, B. J. Shields, Q. Quan, Y. Chu, N. P. de Leon, R. Evans, M. J. Burek, A. S. Zibrov, M. Markham, D. J. Twitchen, H. Park, M. D. Lukin, and M. Lončar, Coupling of NV centers to photonic crystal nanobeams in diamond, Nano Lett. **13**, 5791 (2013).
[30] A. Faraon, C. Santori, Z. Huang, V. M. Acosta, and R. G. Beausoleil, Coupling of Nitrogen-Vacancy Centers to Photonic Crystal Cavities in Monocrystalline Diamond, Phys. Rev. Lett. **109**, 033604 (2012).
[31] P. Siyushev, H. Pinto, M. Vörös, A. Gali, F. Jelezko, and J. Wrachtrup, Optically Controlled Switching of the Charge State of a Single Nitrogen-Vacancy Center in Diamond at Cryogenic Temperatures, Phys. Rev. Lett. **110**, 167402 (2013).
[32] M. W. Doherty, F. Dolde, H. Fedder, F. Jelezko, J. Wrachtrup, N. B. Manson, and L. C. L. Hollenberg, Theory of the ground-state spin of the NV^- center in diamond, Phys. Rev. B **85**, 205203 (2012).
[33] M. W. Doherty, V. V. Struzhkin, D. A. Simpson, L. P. McGuinness, Y. Meng, A. Stacey, T. J. Karle, R. J. Hemley, N. B. Manson, L. C. L. Hollenberg, and S. Prawer, Electronic Properties and Metrology Applications of the Diamond NV^- Center under Pressure, Phys. Rev. Lett. **112**, 047601 (2014).
[34] W. Weaver, S. P. Timoshenko, and D. H. Young, *Vibration Problems in Engineering*, 5th ed. (Wiley, New York, 1990).
[35] K.-M. C. Fu, C. Santori, P. E. Barclay, and R. G. Beausoleil, Conversion of neutral nitrogen-vacancy centers to negatively charged nitrogen-vacancy centers through selective oxidation, Appl. Phys. Lett. **96**, 121907 (2010).
[36] S. Cui, A. S. Greenspon, K. Ohno, B. A. Myers, A. C. Bleszynski Jayich, D. D. Awschalom, and E. L. Hu, Reduced plasma-induced damage to near-surface nitrogen-vacancy centers in diamond, Nano Lett. **15**, 2887 (2015).
[37] Y. Chu, N. P. de Leon, B. J. Shields, B. Hausmann, R. Evans, E. Togan, M. J. Burek, M. Markham, A. Stacey, A. S. Zibrov, A. Yacoby, D. J. Twitchen, M. Lončar, H. Park, P. Maletinsky, and M. D. Lukin, Coherent optical transitions in implanted nitrogen vacancy centers, Nano Lett. **14**, 1982 (2014).
[38] N. de Leon, R. Evans, K. De Greve, M. Goldman, A. High, M. Markham, A. Stacey, D. Twitchen, M. Lončar, H. Park, and M. Lukin, Quantum optics in the solid state with diamond nanophotonics, Bull. Am. Phys. Soc. **60**, 7 (2015).
[39] M. J. Burek, D. Ramos, P. Patel, I. W. Frank, and M. Lončar, Nanomechanical resonant structures in single-crystal diamond, Appl. Phys. Lett. **103**, 131904 (2013).
[40] T. Kouh, D. Karabacak, D. H. Kim, and K. L. Ekinci, Diffraction effects in optical interferometric displacement detection in nanoelectromechanical systems, Appl. Phys. Lett. **86**, 013106 (2005).
[41] L. Childress, M. V. Gurudev Dutt, J. M. Taylor, A. S. Zibrov, F. Jelezko, J. Wrachtrup, P. R. Hemmer, and M. D. Lukin, Coherent dynamics of coupled electron and nuclear spin qubits in diamond, Science **314**, 281 (2006).
[42] Y-I. Sohn, M. J. Burek, and M. Lončar, Dynamic actuation of single-crystal diamond nanobeams, Appl. Phys. Lett. **107**, 243106 (2015).
[43] M. J. Burek, J. D. Cohen, S. M. Meenehan, T. Ruelle, S. Meesala, J. Rochman, O. Painter, and M. Lončar, Diamond optomechanical crystals, arXiv:1512.04166.
[44] M. Imboden and P. Mohanty, Dissipation in nanoelectromechanical systems, Phys. Rep. **534**, 89 (2014).
[45] A. Imamoğlu, Cavity QED Based on Collective Magnetic Dipole Coupling: Spin Ensembles as Hybrid Two-Level Systems, Phys. Rev. Lett. **102**, 083602 (2009).
[46] A. Batalov, V. Jacques, F. Kaiser, P. Siyushev, P. Neumann, L. J. Rogers, R. L. McMurtrie, N. B. Manson, F. Jelezko, and J. Wrachtrup, Low Temperature Studies of the Excited-State Structure of Negatively Charged Nitrogen-Vacancy Color Centers in Diamond, Phys. Rev. Lett. **102**, 195506 (2009).
[47] G. Davies and M. F. Hamer, Optical studies of the 1.945 ev vibronic band in diamond, Proc. R. Soc. A **348**, 285 (1976).
[48] H. Sternschulte, K. Thonke, R. Sauer, P. C. Münzinger, and P. Michler, 1.681-eV luminescence center in chemical-vapor-deposited homoepitaxial diamond films, Phys. Rev. B **50**, 14554 (1994).